Nano Letters, 15, 629 (2015)

Approved for public release

Adsorbate Diffusion on Transition Metal Nanoparticles

Guowen Peng and Manos Mavrikakis*

Department of Chemical and Biological Engineering, University of Wisconsin-Madison, Madison, WI 53706, United States

ABSTRACT: Diffusion of adsorbates on transition metal nanoparticles is a precursor process for heterogeneously catalyzed reactions, and as a result, an atomistic understanding of the diffusion mechanism is very important. We systematically studied adsorption and diffusion of atomic and diatomic species (H, C, N, O, CO, and NO) on nanometer-sized Pt and Cu nanoparticles with different sizes and shapes using density functional theory calculations. We show that nanoparticles bind adsorbates more strongly than the corresponding extended single crystal metal surfaces. We find that there is a Bronsted-Evans-Polanyi type linear correlation between the transition-state energy and the initial-state energy for adsorbate diffusing across the edges of Pt and Cu nanoparticles. We further show that the barrier for adsorbate diffusion across the nanoparticles edges can be estimated by the binding energy of the adsorbate on the nanoparticles. These results provide useful insights for understanding diffusion-mediated chemical reactions catalyzed by transition metal nanoparticles which are widely used in heterogeneous catalysis.

KEYWORDS: Heterogeneous catalysis, diffusion, edge barrier, transition metal nanoparticles, DFT calculations

Diffusion of adsorbed species on transition metal surfaces is an important process for thin-film and nanostructure growth and for heterogeneous catalysis, among others.[1-4] In connection to the latter, such surface diffusion is the precursor process for the subsequent heterogeneously catalyzed reactions, thereby affecting catalytic chemistry.

Nilekar et.al. have shown that the transition state energy for the diffusion of a variety of catalytically relevant adsorbed species on single crystal transition metal surfaces correlates well with the binding energy of the adsorbate on the respective surface.[5] This correlation is a Bronsted-Evans-Polanyi (BEP)-type of correlation, similar to other BEP correlations established earlier for surface-catalyzed bond-breaking/bond-making reactions.[6-9] The universal BEP-type correlation is independent of the nature of the adsorbed species and that of the metal surface. For a certain class of surface-catalyzed reactions, the existence of a BEP-type correlation reflects a similarity between the geometry of the transition state and that of the final state, resulting in a linear relationship with a slope near to unity.[6] Furthermore, for surface diffusion on transition metal surfaces, a rule of thumb on the diffusion barrier was found, i.e., the diffusion barrier can be estimated by ca. 12% of the magnitude of the binding energy of the adsorbate.[5]

Compared with bulk metals and extended metal surfaces, nanometer-sized metal nanoparticles have unique physical and chemical properties. For example, though bulk Au and extended Au surfaces are quite inert,[10] very small Au nanoparticles are active for CO oxidation,[11-15] water-gas-shift reaction,[16] formic acid decomposition,[17,18] and selective oxidation of styrene towards its epoxide.[19] The unique properties of small metal nanoparticles have been generally attributed to the presence of under-coordinated sites (e.g., the bridge and top sites on the edges, the vertex site at the corners), possible quantum-sized effects, specific shape of the nanoparticles, strain developed on their facets, and the interaction between the nanoparticles and their support.[20-26] For transition metal nanoparticles catalyzed reactions, adsorption and diffusion of species on the nanoparticles are important processes; yet, several related questions remain open: (1) How strong do the nanometer-sized transition metal nanoparticles bind the adsorbed species compared to the corresponding extended single crystal metal surfaces? (2) For

diffusion across the edge of nanoparticles, does the BEP-type correlation between, for instance, the transition-state energy and the initial-state energy hold? (3) Is there a way to estimate the energy barrier for crossing the edge of a nanoparticle, where the edge connects two adjacent facets of the nanoparticle, from the binding energy of the adsorbate on a facet of the nanoparticle? The answers to these questions are of paramount importance for understanding the physics and chemistry occurring on the nanoparticles. However, due to the excessive computational cost of nanoparticle modelling through electronic structure theoretical methods, a quantitative study with accurate density functional theory (DFT) calculations is still missing.

Here, we perform a systematic DFT study of the adsorption and diffusion energetics of selected adsorbed species on transition metal nanoparticles. We choose four atomic species and two diatomic molecules (H, C, N, O, CO, and NO) as adsorbates and study the adsorption and diffusion of these adsorbates across the edges of Pt and Cu nanoparticles with different sizes and shapes: 1.07 nm Pt_{55} and 1.62 nm Pt_{147} cuboctahedral nanoparticles, and 0.96 nm Cu_{55} and 1.46 nm Cu_{147} icosahedral nanoparticles. We show that nanoparticles bind adsorbates more strongly than the corresponding extended single crystal surfaces; a BEP-type correlation between the transition-state energy and the initial-state energy holds for these six adsorbates diffusing across the edge of Pt and Cu nanoparticles; and the diffusion barrier across the edge of Pt and Cu nanoparticles can be estimated by the binding energy of the adsorbate on Pt and Cu nanoparticles.

All calculations were performed using the Vienna ab-initio Simulation Package (VASP) code[27,28] based on density functional theory. The projector augmented wave (PAW) potentials[29,30] were used for electron-ion interactions and the generalized gradient approximation (GGA–PW91)[31] was used to describe the exchange-correlation functional. The electron wave function was expanded using plane waves with an energy cutoff of 400 eV. The calculated Pt and Cu lattice constants (3.99 and 3.64 Å, respectively) were used; these values are in good agreement with the respective experimental values (3.92 and 3.62 Å, respectively).[32] The extended Pt(111) and Cu(111) surfaces were modeled by a four-layer slab with a (2×2) unit cell; whereas the open Pt(001) and Cu(001) surfaces were modelled by a six-layer slab in a

(2×2) unit cell. A vacuum layer of ~12 Å was used to separate periodic images along the *z* direction. For Pt, cuboctahedral Pt_{55} and Pt_{147} nanoparticles were used; for Cu, considering the instability of cuboctahedral Cu nanoparticles up to 2000 atoms, icosahedral Cu_{55} and Cu_{147} nanoparticles were selected.[33] The Pt and Cu nanoparticles were modeled by a supercell with 3-dimenisonal periodic boundary conditions in a simple cubic cell. A large vacuum region along each of the three dimensions was used to ensure that the interactions between each nanoparticle and its periodic image are negligible (the distance between two nearest surface atoms in neighbouring images is at least 16 Å). The Brillouin zones of the Pt(111), Cu(111), Pt(001), and Cu(001) surfaces were sampled using a (8×8×1) k-point mesh based on the Monkhorst-Pack scheme.[34] The Brillouin zones of Pt and Cu nanoparticles were sampled by the Gamma point only. The bottom-two layers of Pt(111), Cu(111), Pt(001), Cu(001) were fixed during relaxation. Pt_{55}, Pt_{147}, Cu_{55}, and Cu_{147} nanoparticles were fully relaxed without any constraint. All structures were fully relaxed until the Hellmann-Feynman forces acting on the atoms were smaller than 0.02 eV/Å. The climbing image nudged elastic band (CI-NEB) method[35] was used to calculate the diffusion barriers of adsorbates. The binding energy (BE) is defined as BE= E_{ads} - E_{clean} - E_{gas}, where E_{ads}, E_{clean}, and E_{gas} are the calculated total energies of the slab (nanoparticle) with adsorbate, the clean slab (nanoparticle), and the adsorbate species in the gas phase, respectively.

We first calculated the binding properties of H, C, N, O, CO, and NO on Pt_{55}, Pt_{147}, Cu_{55} and Cu_{147} nanoparticles. On cuboctahedral Pt nanoparticles which expose both (001) and (111) facets, we considered different high symmetry adsorption sites on both (001) and (111) facets: (a) fcc, hcp, bridge (B111) sites on the (111) facet, (b) bridge (B100), top (A100), hollow (hol) sites on the (001) facet, (c) the under-coordinated bridge (BE10) and top (AE10) sites on the edge, and the vertex site (AV) at the corner. On icosahedral Cu nanoparticles which expose (111) facets only, different high symmetry sites on the (111) facet as well as bridge site (BE11) and top site (AE11) on the edge between two adjacent (111) facets, and the vertex site at the corner were considered. These different adsorption sites are schematically shown in Figure 1.

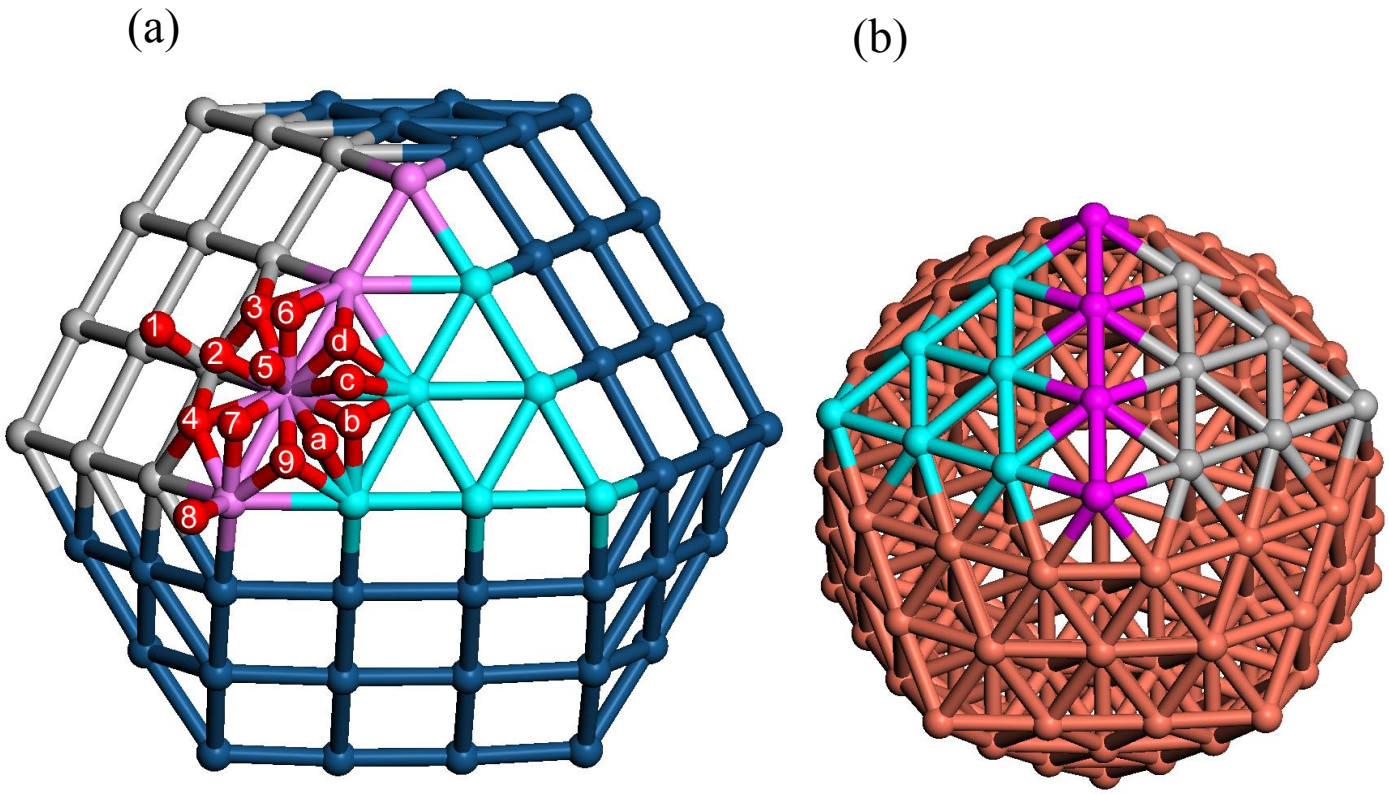

Figure 1. (a) Different adsorption sites on the *cuboctahedral* Pt_{147} nanoparticle (only part of the outermost shell of atoms is shown): (1) A100: top site on the (001) facet. (2) B100: bridge site on the (001) facet. (3) hol-side: hollow site (middle) on the (001) facet. (4) hol: hollow site (corner) on the (001) facet. (5) AE10: top site at the edge between (001) and (111) facets. (6) BE10-b: bridge site (middle) at the edge between (001) and (111) facets. (7) BE10-a: bridge site (corner) at the edge between (001) and (111) facets. (8) AV: vertex site. (9) hcp-a: hcp site (corner) on the (111) facet. (a) B111-a: bridge site (close to corner) on the (111) facet. (b) fcc site on (111) facet. (c) B111-b: bridge site (middle) on the (111) facet. (d) hcp-b: hcp site (middle) on the (111) facet. Red and blue spheres denote adsorbates and Pt atoms. Pt atoms on one (001) facet, one (111) facet, and the edge between them are highlighted by grey, cyan, and pink spheres, respectively. (b) For *icosahederal* Cu_{147} nanoparticle, only adsorption sites on the (111) facet, on the edge, and at the vertex are available. The notations of BE10 and AE10 are changed to BE11 and AE11, respectively.

Summarized in Table 1 are the most favorable adsorption sites and the calculated binding energies for H, C, N, O, CO, and NO on the Pt and Cu nanoparticles examined here. For comparison, we also

calculated the binding energy for these adsorbates on the flat Pt(111), Pt(001), Cu(111), and Cu(001) surfaces and the respective data are also included in Table 1. As it is clearly seen from Table 1, on the single crystal close-packed (111) surfaces, the fcc site is the most favorable for all six adsorbates studied; whereas on the open single crystal (001) surfaces, the bridge and hollow sites are favorable. Note that as a general trend, the open (001) surfaces bind adsorbates more strongly than the close-packed (111) surfaces, primarily because metal atoms have lower coordination numbers on the (001) surfaces.

On nanoparticles, much more diversified trends were found. On the *cuboctahedral* Pt nanoparticles, and for H, O, CO, and NO, the under-coordinated bridge site at the edge (BE10) and the bridge site on the (001) facet (B100) are very stable. For H on Pt_{55} (denoted as H/Pt_{55}—similar notations will be used thereafter), the most stable site is B100, with a binding energy (BE) of -3.05 eV. The BE10 site is slightly less stable, with a binding energy of -2.94 eV, identical to the binding energy of H on the flat Pt(001) surface. For O/Pt_{55}, the BE10 site is the most stable, with a binding energy of -4.75 eV, followed by the hcp site on the (111) facet with a binding energy of -4.60 eV. For CO/Pt_{55}, the binding energy on B100, AV, BE10, AE10 is -2.44, -2.42, -2.23, -2.24 eV, respectively, all stronger than that of CO on the flat Pt(001) surface (BE = -2.11 eV). For NO/Pt_{55}, the binding energy on B100, BE10, and AV is -2.61, -2.56, -2.56 eV, respectively. We note in passing that the BE10-b site (the middle bridge site on the edge) is the most favorable for H/Pt_{147}, O/Pt_{147}, CO/Pt_{147}, and NO/Pt_{147}, with a binding energy of -3.04, -4.66, -2.32, and -2.54 eV, respectively. The hcp site near the corner is the most stable site for N/Pt_{55} and N/Pt_{147}, with a binding energy of -5.37 and -5.02 eV, respectively. For C/Pt_{55} and C/Pt_{147}, the four-fold hollow site on (001) is the most favorable, with a binding energy of -7.79 and -7.90 eV, respectively. As a comparison, the hollow site on the flat Pt(001) is the most stable adsorption site for C, with a binding energy of -7.71 eV.

Table 1. The most favorable binding site and binding energy (BE, in eV) for H, C, N, O, CO, NO adsorbed on Pt_{55}, Pt_{147}, Cu_{55}, Cu_{147} nanoparticles. Data on Pt(111), Pt(001), Cu(111), and Cu(001) single crystal surfaces are also included for comparison.

System	Site[a]	BE	System	Site[a]	BE
H/Pt_{55}	B100	-3.05	H/Cu_{55}	fcc	-2.68
C/Pt_{55}	hol	-7.79	C/Cu_{55}	4-fold[b]	-5.66
N/Pt_{55}	hcp	-5.37	N/Cu_{55}	hcp	-4.32
O/Pt_{55}	BE10	-4.75	O/Cu_{55}	hcp	-5.19
CO/Pt_{55}	B100	-2.44	CO/Cu_{55}	hcp	-1.19
NO/Pt_{55}	B100	-2.61	NO/Cu_{55}	hcp	-1.67
H/Pt_{147}	BE10-b	-3.04	H/Cu_{147}	hcp-b	-2.49
C/Pt_{147}	hol	-7.90	C/Cu_{147}	4-fold[b]	-5.26
N/Pt_{147}	hcp-a	-5.02	N/Cu_{147}	hcp-a	-3.94
O/Pt_{147}	BE10-b	-4.66	O/Cu_{147}	hcp-a	-5.14
CO/Pt_{147}	B100-b	-2.37	CO/Cu_{147}	AV	-0.88
NO/Pt_{147}	BE10-b	-2.54	NO/Cu_{147}	hcp-a	-1.27
H/Pt(111)	fcc	-2.77	H/Cu(111)	fcc	-2.53
C/Pt(111)	fcc	-7.05	C/Cu(111)	fcc	-4.83
N/Pt(111)	fcc	-4.82	N/Cu(111)	fcc	-3.73
O/Pt(111)	fcc	-4.39	O/Cu(111)	fcc	-4.79
CO/Pt(111)	fcc	-1.76	CO/Cu(111)	fcc	-0.92
NO/Pt(111)	fcc	-1.96	NO/Cu(111)	fcc	-1.22
H/Pt(001)	bri	-2.94	H/Cu(001)	hol	-2.41
C/Pt(001)	hol	-7.71	C/Cu(001)	hol	-6.19
N/Pt(001)	hol	-4.58	N/Cu(001)	hol	-4.61
O/Pt(001)	bri	-4.30	O/Cu(001)	hol	-5.11
CO/Pt(001)	bri	-2.11	CO/Cu(001)	bri	-0.82
NO/Pt(001)	bri	-2.33	NO/Cu(001)	hol	-1.28

[a] See Fig. 1 for notation of different adsorption sites.
[b] Pseudo-four-fold site developed from the distortion of the local (111) facet.

On the *icosahedral* Cu nanoparticles, we found that the hcp site near the corner (hcp-a shown in Fig. 1) is very stable. On the smaller Cu_{55} nanoparticle, the most favorable site is the hcp site near the corner (hcp-a) for N, O, CO, and NO. For H/Cu_{55}, the fcc site is 0.13 eV more stable than the hcp site. Interestingly, for C/Cu_{55}, we found that C placed at hcp, AE11, and BE11 sites as initial guess to the energy minimization procedure, always relaxes to pseudo-four-fold hollow sites by relaxing the underneath Cu atoms to a localized square-like Cu(001) geometry—a tendency to form four-fold coordinated C as on the flat Cu(001) surface. On the larger Cu_{147} nanoparticle, H, N, O, and NO all prefer the hcp sites. For CO/Cu_{147}, we find that the vertex site (AV) and edge sites (BE11 and AE11) are slightly more stable than the hcp sites. Similarly to C/Cu_{55}, for C/Cu_{147}, the pseudo-four-fold hollow site, which developed by distorting the local (111) facet, is the most stable site.

By comparing the binding energy of different adsorbates on Pt and Cu nanoparticles and the corresponding single crystal extended surfaces shown in Table 1, we found that nanoparticles bind adsorbates more strongly. Compared with the single crystal close-packed (111) surface, the 1.07 nm-sized cuboctahedral Pt_{55} nanoparticle binds H, C, N, O, CO, and NO stronger by 0.28, 0.74, 0.55, 0.36, 0.68, and 0.65 eV, respectively. Compared with the single crystal open Pt(001) surface, the Pt_{55} nanoparticle, binds H, C, N, O, CO, and NO more strongly by 0.11, 0.08, 0.79, 0.45, 0.33, and 0.28 eV, respectively. The increase in binding strength on nanoparticles can be attributed to the presence of under-coordinated sites on the nanoparticles. Indeed, the single crystal Pt(001) surface (with a coordination number of 8 for its surface metal atoms) binds adsorbates more strongly in general than the close-packed Pt(111) surface (with a coordination number of 9 for its surface metal atoms). On Pt nanoparticles, the edge and vertex sites of nanoparticles have even smaller coordination numbers (7 and 5 respectively), and thus tend to bind adsorbates more strongly.

On the larger 1.46-nm sized Pt_{147} nanoparticle, the binding strength increase with respect to single crystal surfaces is less pronounced than that found on the smaller Pt_{55} nanoparticle. Compared with the single crystal close-packed (111) surface, Pt_{147} binds H, C, N, O, CO, and NO more strongly by 0.27, 0.85, 0.19, 0.27, 0.61, and 0.58 eV, respectively. With the binding energy on single crystal Pt(001) as the

reference, on Pt_{147} the binding strength of H, C, N, O, CO, and NO increases by 0.10, 0.20, 0.44, 0.36, 0.26, and 0.21 eV, respectively. The stronger binding on the smaller nanoparticles can be understood by the finite size effect.[22,24-26] As the diameter of nanoparticles increases, their properties can be viewed as converging to the respective single crystal limits.[22]

Similar trends are found for adsorption on the icosahedral Cu nanoparticles which expose only (111) facets. Compared to the single crystal close-packed Cu(111), the smaller 0.96-nm sized Cu_{55} particle binds H, C, N, O, CO, and NO more strongly by 0.15, 0.83, 0.59, 0.40, 0.27 and 0.45 eV, respectively. The larger 1.64-nm sized Cu_{147} nanoparticle, the binding strength increases by 0.43, 0.21, 0.35 eV for C, N, and O respectively; whereas the binding energy changes for H, CO, and NO is very small. We note in passing that the flat Cu(001) surface binds C more strongly than both Cu nanoparticles. This is because icosahedral Cu nanoparticles do not contain four-fold hollow sites which optimize the four-fold coordination for C. The stronger binding on the smaller nanoparticles than on the larger ones can be explained by the particle size effect.[22,24-26]

Having calculated the binding trends of these adsorbates on Pt and Cu nanoparticles, we now study adsorbate diffusion across the edge of the nanoparticles. On Pt cuboctahedral nanoparticles, all possible diffusion paths across the edge from the (001) facet to the neighbouring (111) facet were investigated; while on Cu icosahedral nanoparticles, all possible diffusion paths across the edge between two adjacent (111) facets were analyzed. After comparing different diffusion paths for each adsorbate, the minimum energy path (MEP) across the edge of the nanoparticles was determined on both Pt and Cu nanoparticles. Representative examples of the MEPs for NO diffusion across the edge of cuboctahedral Pt_{147} and icosahedral Cu_{147} nanoparticles are shown in Figure 2. The rate-determining step (RDS) of the diffusion across the edge was then identified as the step along the diffusion reaction coordinate characterized by the largest activation energy barrier, and the initial-state energy (BE_{IS}), transition-state energy (BE_{TS}), and edge barrier (E_{edge}, defined as BE_{TS} - BE_{IS}) were obtained. For example, for NO diffusion across the edge of Pt_{147} nanoparticle, the RDS is from the bridge site at the edge between (001) and (111) facets (BE10-b) to the hcp site (hcp-b) on the (111) facet, with BE_{IS}, BE_{TS} and E_{ES} of -2.54, -2.01, and 0.53 eV, respectively. The complete dataset for 24 adsorbate-nanoparticle pairs is tabulated in Table 2. A close look at Table 2 reveals that almost all the RDS for the adsorbates diffusion starts from or ends at the bridge sites at the edge connecting adjacent facets except for: (i) H on Pt_{55} and Pt_{147} where the RDS ends with the top site on the edge, (ii) C/Cu_{55} where the RDS is from one pseudo-four-fold hollow site derived from the hcp site to another pseudo-four-fold site at the edge derived from the BE11 site, and (iii) O on Cu_{55} and Cu_{147} where the RDS is from one hcp site to another hcp site in the adjacent (111) facet.

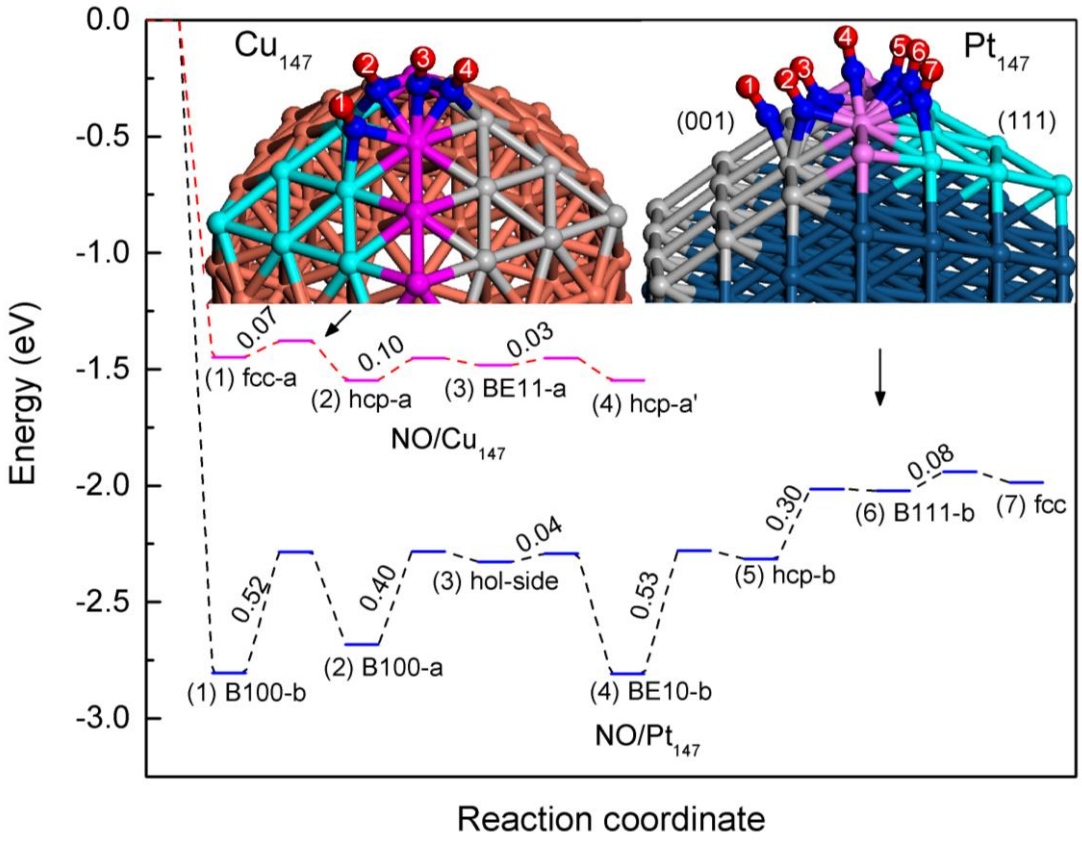

Figure 2. Potential energy surface for NO diffusion across the edge of cuboctahedral Pt_{147} nanoparticle (blue line) and icosahedral Cu_{147} nanoparticle (red line). The atomic strucures are schematically shown in the inset: Pt_{147} on the right, Cu_{147} on the left. Blue sphere is N, and red sphere is O atom. The energy is refrenced to the total energies of clean nanoparticle and gas phase NO.

Table 2. Binding Energy of the initial-state (BE_{IS}) and transition-state (BE_{TS}) for diffusion across the edge of nanoparticles for different adsorbates. The TS corresponds to the rate determining step (RDS). E_{edge} gives the activation energy barrier for that diffusion event. All energies are in eV.

System	RDS	BE_{IS}	BE_{TS}	E_{edge}
H/Pt_{55}	B100 → AE10	-3.05	-2.81	0.24
C/Pt_{55}	hcp → hol	-7.75	-6.72	1.03
N/Pt_{55}	hcp → BE10	-5.37	-4.77	0.60
O/Pt_{55}	BE10 → B100	-4.75	-4.14	0.61
CO/Pt_{55}	B100→ AE10	-2.44	-2.03	0.41
NO/Pt_{55}	BE10 → hol-side	-2.56	-1.87	0.68
H/Pt_{147}	BE10-b → AE10	-3.04	-2.80	0.24
C/Pt_{147}	hol-side → BE10-b	-7.72	-6.68	1.04
N/Pt_{147}	hcp-a→ BE10-a	-5.02	-4.39	0.63
O/Pt_{147}	BE10-b → hcp-b	-4.66	-4.24	0.42
CO/Pt_{147}	BE10-b → hcp-b	-2.32	-1.97	0.35
NO/Pt_{147}	BE10-b → hcp-b	-2.54	-2.01	0.53
H/Cu_{55}	hcp → BE11	-2.55	-2.39	0.16
C/Cu_{55}	4-fold → 4-fold-b[a]	-5.66	-5.19	0.47
N/Cu_{55}	hcp → BE11	-4.32	-3.92	0.40
O/Cu_{55}	hcp → hcp' [b]	-5.19	-4.60	0.59
CO/Cu_{55}	hcp → BE11	-1.10	-0.96	0.14
NO/Cu_{55}	hcp → BE11	-1.67	-1.36	0.31
H/Cu_{147}	hcp-b → BE11-b	-2.49	-2.44	0.05
C/Cu_{147}	hcp-b → BE11-b	-5.24	-4.89	0.35
N/Cu_{147}	hcp-b → BE11-b	-3.92	-3.79	0.13
O/Cu_{147}	hcp-a → hcp-a' [b]	-5.14	-4.61	0.53
CO/Cu_{147}	BE-b → hcp-b	-0.82	-0.76	0.06
NO/Cu_{147}	hcp-a → BE11-a	-1.27	-1.18	0.10

[a] Pseudo-four-fold hollow site at the edge close to the corner. [b] hcp site in the adjacent (111) facet.

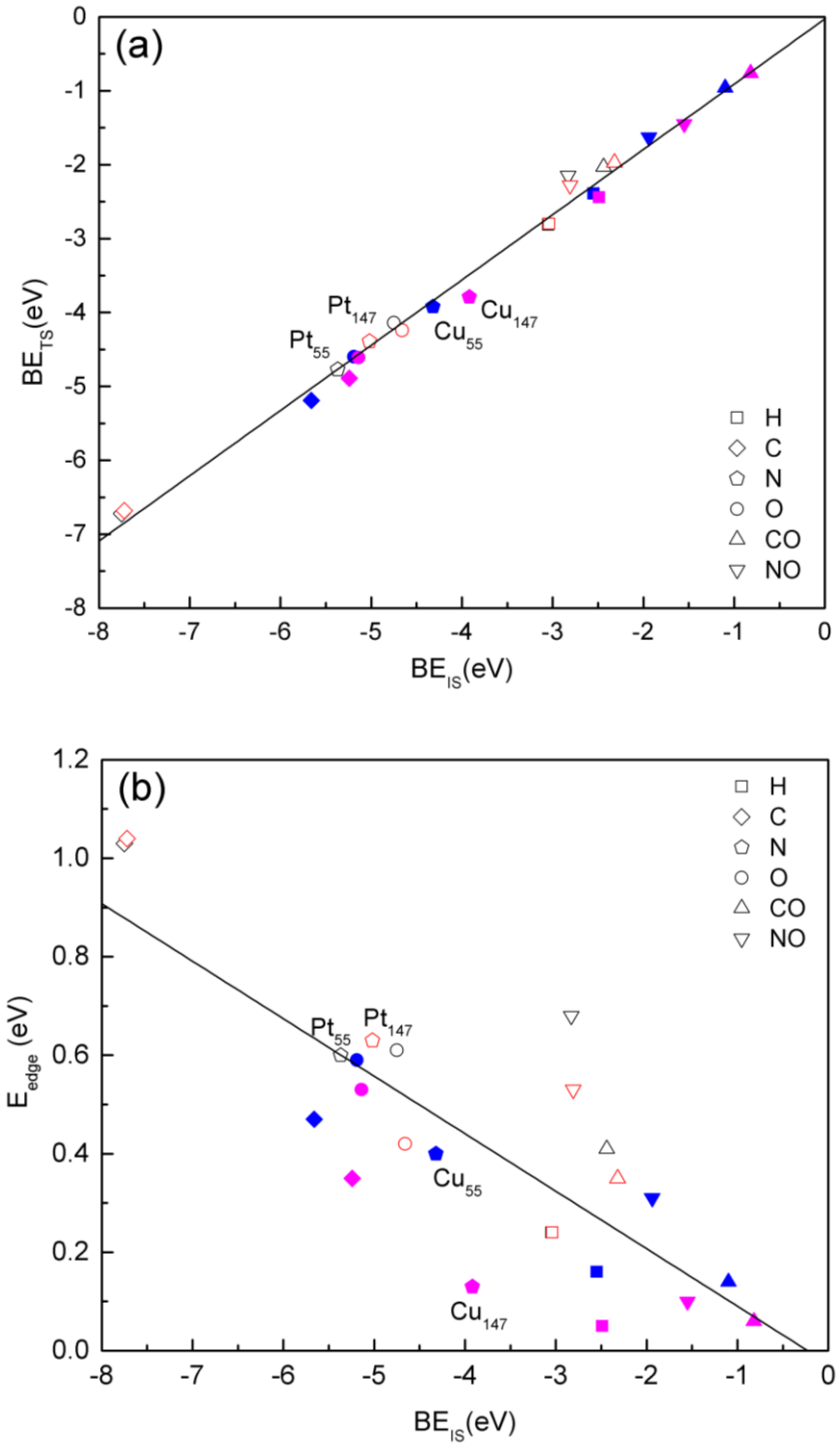

Figure 3. (a) Binding energy of the transition state (BE_{TS}) versus binding energy of the initial state (BE_{IS}) for the rate-determing-step of adsorbate diffusion across the edge of the Pt and Cu nanoparticles. Data shown with empty symbols are for Pt nanoparticles (Pt_{55} black, Pt_{147} red). Data shown with filled symbols are for Cu nanoparticles (Cu_{55} blue and Cu_{147} magenta). The best fit line gives BE_{TS} = -0.03 + 0.88 BE_{IS} with R^2=0.99. (b) The barrier over the edge (E_{edge}) plotted against the binding energy of the initial state (BE_{IS}) for the RDS of adsorbate across the edge. The linear regression gives E_{edge} = -0.03 - 0.12 BE_{IS} with R^2=0.66.

We next examine the relation between the transition-state energy and the initial state energy of the RDS of all 24 data points. Plotted in Figure 3(a) is the transition-state energy BE_{TS} as a function of the initial-state energy BE_{IS}. Remarkably, there is a good BEP-type correlation between BE_{TS} and BE_{IS}: the best fit line gives BE_{TS} (eV) = -0.004 + 0.89 BE_{IS} with R^2=0.99. For comparison, on Pt(111) and Cu(111) surfaces, the correlation between BE_{TS} and BE_{IS} is BE_{TS} = -0.10 + 0.87 BE_{IS} with R^2=0.99. This result suggests that a great similarity exists between the energetics of diffusion events on small metal nanoparticles and on single crystal surfaces, leading to a nearly universal description capable of accounting for surface diffusion on both classes of surfaces.

Finally, we turn our attention to address the question on estimating the barrier for adsorbates to cross the edge on nanoparticles from the binding energy of the adsorbates. From this present work, on the single crystal Pt(111) and Cu(111) surfaces, the correlation between the diffusion barrier E_a and the binding energy of the adsorbate BE_{IS} is E_a = -0.11 - 0.13 BE_{IS} with R^2=0.60, which is close to the best fit line reported previously.[5] For adsorbate diffusing across the edge of nanoparticles, we plotted the edge barrier E_{edge} as a function of the initial-state energy BE_{IS} in Figure 3(b) and fitted the data using linear regression. Though scatter around the best fit line exists, the edge barrier E_{edge} can be correlated with the binding energy BE_{IS} of the adsorbates via E_{edge} = -0.003 - 0.11 BE_{IS} with R^2=0.62, i.e., the edge barrier E_{edge} can be roughly estimated as equal to 11% of the initial-state energy BE_{IS}. This indicates that the rule of thumb on surface diffusion barrier on single crystal transition metal surfaces can be generalized to adsorbate diffusion across the edge connecting adjacent facets on transition metal nanoparticles.

In summary, we presented a systematic density functional theory study on adsorbate adsorption on two small nanoparticles of Pt and Cu and diffusion of those species across the edge of these nanoparticles. We showed that on Pt and Cu nanoparticles, adsorbates (H, C, N, O, CO, and NO) bind more strongly than on the respective single crystal surfaces, mainly because of the presence of under-coordinated sites on the nanoparticles. Size of the nanoparticles was also shown to play a role in determining adsorbates' binding energies on the nanoparticles. Remarkably, we found that for adsorbate diffusing across an edge of the nanoparticles, a universal Bronsted-Evans-Plonyi-type correlation between the transition-state energy and

the initial-state energy holds. Furthermore, we showed that one can estimate the diffusion barrier for adsorbates crossing a Cu or Pt nanoparticle's edge by ~11% of the binding energy of the adsorbates at the initial state of the diffusion rate-determining-step.

AUTHOR INFORMATION

Corresponding Author

*E-mail: manos@engr.wisc.edu

Notes

The authors declare no competing financial interest.

ACKNOWLEDGEMENTS

This work was supported by DOE-BES, Division of Chemical Sciences (grant DE-FG02-05ER15731), and by the Air Force Office of Scientific Research under a Basic Research Initiative grant (AFOSR FA9550-12-1-0481). Supercomputer time at National Energy Research Scientific Computing Center (NERSC), Pacific Northwest National Laboratory (PNNL), and Argonne National Laboratory (ANL), all supported by the DOE, is greatly appreciated. Additional CPU resources at the DoD High Performance Computing Modernization Program (US Air Force Research Laboratory DoD Supercomputing Resource Center (AFRL DSRC), the US Army Engineer Research and Development Center (ERDC), and the Navy DoD Supercomputing Resource Center (Navy DSRC)) supported by the Department of Defence, were used to conduct this work.

REFERENCES

(1) Renisch, S.; Schuster, R.; Wintterlin, J.; Ertl, G. *Phys. Rev. Lett.* 1999, *82*, 3839.

(2) Horch, S.; Lorensen, H. T.; Helveg, S.; Laegsgaard, E.; Stensgaard, I.; Jacobsen, K. W.; Norskov, J. K.; Besenbacher, F. *Nature* 1999, *398*, 134.

(3) Evans, J. W.; Thiel, P. A.; Bartelt, M. C. *Surf. Sci. Rep.* 2006, *61*, 1.

(4) Mo, Y. N.; Zhu, W. G.; Kaxiras, E.; Zhang, Z. Y. *Phys. Rev. Lett.* 2008, *101*, 4.

(5) Nilekar, A. U.; Greeley, J.; Mavrikakis, M. *Angew. Chem.-Int. Edit.* 2006, *45*, 7046.

(6) Norskov, J. K.; Bligaard, T.; Logadottir, A.; Bahn, S.; Hansen, L. B.; Bollinger, M.; Bengaard, H.; Hammer, B.; Sljivancanin, Z.; Mavrikakis, M.; Xu, Y.; Dahl, S.; Jacobsen, C. J. H. *J. Catal.* 2002, *209*, 275.

(7) Greeley, J.; Mavrikakis, M. *Nat. Mater.* 2004, *3*, 810.

(8) Xu, Y.; Ruban, A. V.; Mavrikakis, M. *J. Am. Chem. Soc.* 2004, *126*, 4717.

(9) Bligaard, T.; Norskov, J. K.; Dahl, S.; Matthiesen, J.; Christensen, C. H.; Sehested, J. *J. Catal.* 2004, *224*, 206.

(10) Hammer, B.; Norskov, J. K. *Nature* 1995, *376*, 238.

(11) Iizuka, Y.; Fujiki, H.; Yamauchi, N.; Chijiiwa, T.; Arai, S.; Tsubota, S.; Haruta, M. *Catal. Today* 1997, *36*, 115.

(12) Haruta, M. *Nature* 2005, *437*, 1098.

(13) Valden, M.; Lai, X.; Goodman, D. W. *Science* 1998, *281*, 1647.

(14) Remediakis, I. N.; Lopez, N.; Norskov, J. K. *Angew. Chem.-Int. Edit.* 2005, *44*, 1824.

(15) Herzing, A. A.; Kiely, C. J.; Carley, A. F.; Landon, P.; Hutchings, G. J. *Science* 2008, *321*, 1331.

(16) Fu, Q.; Saltsburg, H.; Flytzani-Stephanopoulos, M. *Science* 2003, *301*, 935.

(17) Ojeda, M.; Iglesia, E. *Angew. Chem.-Int. Edit.* 2009, *48*, 4800.

(18) Singh, S.; Li, S.; Carrasquillo-Flores, R.; Alba-Rubio, A. C.; Dumesic, J. A.; Mavrikakis, M. *Aiche Journal* 2014, *60*, 1303.

(19) Turner, M.; Golovko, V. B.; Vaughan, O. P. H.; Abdulkin, P.; Berenguer-Murcia, A.; Tikhov, M. S.; Johnson, B. F. G.; Lambert, R. M. *Nature* 2008, *454*, 981.

(20) Xia, Y. N.; Xiong, Y. J.; Lim, B.; Skrabalak, S. E. *Angew. Chem.-Int. Edit.* 2009, *48*, 60.

(21) Kleis, J.; Greeley, J.; Romero, N. A.; Morozov, V. A.; Falsig, H.; Larsen, A. H.; Lu, J.; Mortensen, J. J.; Dulak, M.; Thygesen, K. S.; Norskov, J. K.; Jacobsen, K. W. *Catal. Lett.* 2011, *141*, 1067.

(22) Li, L.; Larsen, A. H.; Romero, N. A.; Morozov, V. A.; Glinsvad, C.; Abild-Pedersen, F.; Greeley, J.; Jacobsen, K. W.; Norskov, J. K. *J. Phys. Chem. Lett.* 2013, *4*, 222.

(23) An, W.; Liu, P. *J. Phys. Chem. C* 2013, *117*, 16144.

(24) Han, B. C.; Miranda, C. R.; Ceder, G. *Phys. Rev. B* 2008, *77*, 075410.

(25) Calle-Vallejo, F.; Martinez, J. I.; Garcia-Lastra, J. M.; Sautet, P.; Loffreda, D. *Angew. Chem.-Int. Edit.* 2014, *53*, 8316.

(26) Peterson, A. A.; Grabow, L. C.; Brennan, T. P.; Shong, B.; Ooi, C.; Wu, D. M.; Li, C. W.; Kushwaha, A.; Medford, A. J.; Mbuga, F.; Li, L.; Norskov, J. K. *Topics in Catalysis* 2012, *55*, 1276.

(27) Kresse, G.; Furthmuller, J. *Phys. Rev. B* 1996, *54*, 11169.

(28) Kresse, G.; Furthmuller, J. *Comput. Mater. Sci.* 1996, *6*, 15.

(29) Blochl, P. E. *Phys. Rev. B* 1994, *50*, 17953.

(30) Kresse, G.; Joubert, D. *Phys. Rev. B* 1999, *59*, 1758.

(31) Perdew, J. P.; Wang, Y. *Phys. Rev. B* 1992, *45*, 13244.

(32) *CRC Handbook of Chemistry and Physics, 76th ed.*; CRC Press: New York, 1996.

(33) Valkealahti, S.; Manninen, M. *Phys. Rev. B* 1992, *45*, 9459.

(34) Monkhorst, H. J.; Pack, J. D. *Phys. Rev. B* 1976, *13*, 5188.

(35) Henkelman, G.; Uberuaga, B. P.; Jonsson, H. *J. Chem. Phys.* 2000, *113*, 9901.

Graphic Table of Contents